Chapter 7
The Electromagnetic–Thermal Dosimetry Model of the Human Brain

Mario Cvetković and Dragan Poljak

Abstract The electromagnetic–thermal dosimetry model for the human brain exposed to EM radiation is developed. The electromagnetic (EM) model based on the surface integral equation (SIE) formulation is derived using the equivalence theorem for the case of a lossy homogeneous dielectric body. The thermal dosimetry model of the brain is based on the form of Pennes' equation of heat transfer in biological tissue. The numerical solution of the EM model is carried using the Method of Moments (MoM) while the bioheat equation is solved using the finite element method. Developed electromagnetic thermal model has been applied in internal dosimetry of the human brain to assess the absorbed electromagnetic energy and consequent temperature rise due to exposure of 900 MHz plane wave.

Keywords Electromagnetic-thermal model · Human brain · Numerical dosimetry · Surface integral equation approach

7.1 Introduction

The exposure of a modern man to artificially generated EM fields has raised some controversies as well as unanswered questions regarding the potentially harmful effects on the human health. This is, in particular, the case for the human head and brain exposed to radiation of nowadays ubiquitous cellular phones and base station antennas. Due to this fact the set of techniques for measuring and for calculation of the absorbed EM radiation in the human body referred to as the electromagnetic dosimetry have been developed.

M. Cvetković (✉)
Department of Power Engineering, University of Split, FESB,
R. Boskovica 32, 21000 Split, Croatia
e-mail: mcvetkov@fesb.hr

D. Poljak
Department of Electronics, University of Split, FESB,
R. Boskovica 32, 21000 Split, Croatia
e-mail: dpoljak@fesb.hr

S. Silvestrov and M. Rančić (eds.), *Engineering Mathematics I*,
Springer Proceedings in Mathematics & Statistics 178,
DOI 10.1007/978-3-319-42082-0_7

It is a well established fact that the principal biological effect of high frequency EM radiation is predominantly thermal in nature [1, 10, 12]. If the body absorbs high enough dose of EM power, it could lead to the harmful effects due to a breakdown of the protective thermoregulatory mechanisms. These can be quantified by the analysis of the thermal response of the particular body organ [17].

A direct experimental measurement of the brain thermal response in humans is not possible, and the indirect methods such as magnetic resonance imaging cannot record fine variations in temperature, hence lacking necessary resolution. On the other hand, animal studies are questionable due to a difference in interspecies size and tissue parameters. Consequently, the computational modeling provides the powerful alternative.

This paper describes an electromagnetic–thermal dosimetry model of the human brain. In the first part the electromagnetic model based on the SIE formulation is derived by using the equivalence theorem and the appropriate boundary conditions for the case of lossy dielectric object of an arbitrary shape. The second part outlines the thermal dosimetry model of the human brain based on the form of Pennes' equation of heat transfer in biological tissue. The obtained numerical results for the electric and magnetic fields, respectively, on the brain surface are presented, as well as the distribution of specific absorption rate (SAR) and the related temperature increase.

7.2 Electromagnetic Dosimetry Model

The human brain exposed to incident EM radiation is treated as a classical scattering problem.

The human brain, represented by an arbitrary shape S of a complex parameters (ε_2, μ_2) is placed in a free space with given properties (ε_1, μ_1), as shown in Fig. 7.1a. The complex permittivity of the brain is given by

$$\varepsilon_2 = \varepsilon_0 \varepsilon_r - j\frac{\sigma}{\omega}, \tag{7.1}$$

where ε_0 is permittivity of the free space, ε_r is relative permittivity, σ is electrical conductivity of the brain, and $\omega = 2\pi f$ is the operating frequency. The value for the permeability of the brain is that of free space, i.e. $\mu_0 = 4\pi \times 10^{-7}$ Vs/Am, due to the fact that biological tissues do not posses magnetic properties.

The lossy homogeneous object representing the human brain is exposed to the electromagnetic field $(\mathbf{E}^{inc}, \mathbf{H}^{inc})$. This incident field is present regardless of the scattering object. Due to the scattering object, a scattered field denoted by $(\mathbf{E}^{sca}, \mathbf{H}^{sca})$ is also present. The electric and magnetic fields exterior and interior to the surface S are, $(\mathbf{E}_1, \mathbf{H}_1)$ and $(\mathbf{E}_2, \mathbf{H}_2)$, respectively.

Applying the equivalence theorem, the equivalent problems for both regions 1 and 2 are formulated in terms of the equivalent electric and magnetic current densities $\mathbf{J}$

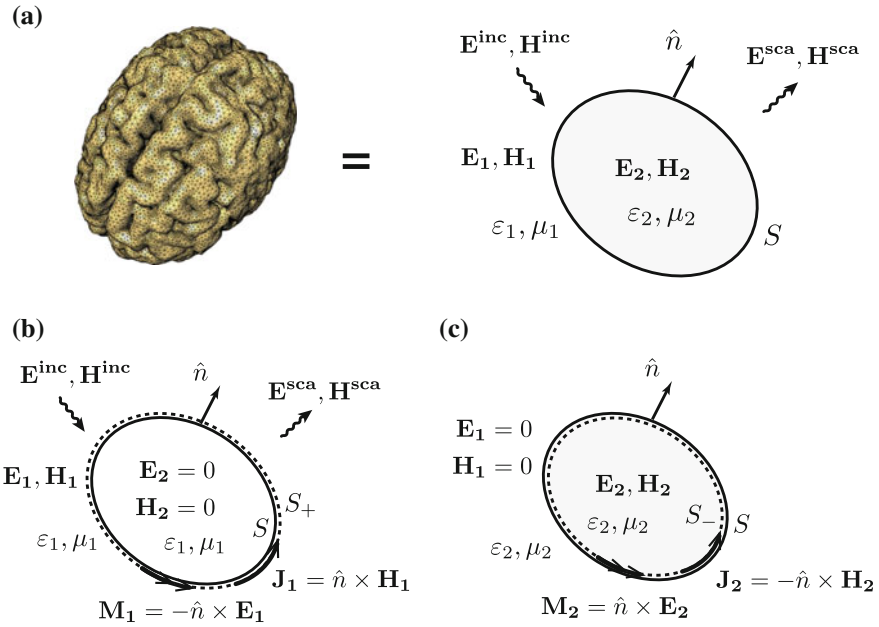

Fig. 7.1 Scattering from arbitrarily shaped lossy homogeneous dielectric (human brain) placed in the incident field ($\mathbf{E}^{inc}$, $\mathbf{H}^{inc}$). **a** Original problem, **b** Region 1 equivalent problem, **c** Region 2 equivalent problem

and $\mathbf{M}$ placed on the scatterer surface S [3, 9, 16, 22]. Two equivalent problems are shown on Fig. 7.1b and c, for the external and internal region, respectively.

In case of region 1 equivalent problem, shown in Fig. 7.1b, the field inside is assumed zero, ($\mathbf{E}_2 = 0, \mathbf{H}_2 = 0$), allowing one to arbitrarily choose material properties for this region. Selecting the properties of the exterior region, a homogeneous domain of (ε_1, μ_1) is obtained, enabling the use of the free space Green's function. The boundary conditions on the surface S are satisfied by introducing the equivalent surface currents $\mathbf{J}_1$ and $\mathbf{M}_1$ at the surface S. Applying the same procedure for the region 2, it follows another homogeneous domain of (ε_2, μ_2). Here as well, the equivalent surface currents $\mathbf{J}_2 = -\mathbf{J}_1$ and $\mathbf{M}_2 = -\mathbf{M}_1$, as shown in Fig. 7.1c, are introduced at the surface S.

Since both equivalent problems represent the equivalent current densities radiating in a homogeneous medium, following expressions for the scattered fields due to these sources can be used:

$$\mathbf{E}_n^{sca}(\mathbf{J}, \mathbf{M}) = -j\omega\mathbf{A}_n - \nabla\varphi_n - \frac{1}{\varepsilon_n}\nabla \times \mathbf{F}_n, \tag{7.2}$$

$$\mathbf{H}_n^{sca}(\mathbf{J}, \mathbf{M}) = -j\omega\mathbf{F}_n - \nabla\psi_n + \frac{1}{\mu_n}\nabla \times \mathbf{A}_n, \tag{7.3}$$

where $n = 1, 2$ is index of the medium where equivalent surface currents radiate, and φ, $\mathbf{F}$, ψ i $\mathbf{A}$ are electric and magnetic, scalar and vector potentials, respectively. These potentials are given in terms of integrals over the sources, i.e.

$$\mathbf{A}_n(\mathbf{r}) = \mu_n \int_S \mathbf{J}(\mathbf{r}\,')G_n(\mathbf{r}, \mathbf{r}\,')\,\mathrm{d}S', \tag{7.4}$$

$$\mathbf{F}_n(\mathbf{r}) = \varepsilon_n \int_S \mathbf{M}(\mathbf{r}\,')G_n(\mathbf{r}, \mathbf{r}\,')\,\mathrm{d}S', \tag{7.5}$$

$$\varphi_n(\mathbf{r}) = \frac{j}{\omega\varepsilon_n} \int_S \nabla'_S \cdot \mathbf{J}(\mathbf{r}\,')G_n(\mathbf{r}, \mathbf{r}\,')\,\mathrm{d}S', \tag{7.6}$$

$$\psi_n(\mathbf{r}) = \frac{j}{\omega\mu_n} \int_S \nabla'_S \cdot \mathbf{M}(\mathbf{r}\,')G_n(\mathbf{r}, \mathbf{r}\,')\,\mathrm{d}S', \tag{7.7}$$

where the electric and magnetic charge from (7.6) and (7.7) is replaced with the divergence of the electric and magnetic current, respectively, featuring the use of a continuity equation. $G_n(\mathbf{r}, \mathbf{r}\,')$ is homogeneous medium Green's function given by

$$G_n(\mathbf{r}, \mathbf{r}\,') = \frac{e^{-jk_nR}}{4\pi R}, \quad R = |\mathbf{r} - \mathbf{r}\,'|, \tag{7.8}$$

where R is the distance from the observation point $\mathbf{r}$ to the source point $\mathbf{r}\,'$, and k_n is the wave number in medium n.

Applying the boundary conditions for the electric field at the interface of the two equivalent problems, i.e. the surface S, the following is obtained

$$\left[-\mathbf{E}_n^{sca}(\mathbf{J}, \mathbf{M})\right]_{tan} = \begin{cases} \left[\mathbf{E}^{inc}\right]_{tan} & , \mathrm{n} = 1, \\ 0 & , \mathrm{n} = 2. \end{cases} \tag{7.9}$$

Equation (7.9) represents the electric field integral equation (EFIE) formulation in the frequency domain for the lossy homogeneous object, i.e. the human brain. The incident field $\mathbf{E}^{inc}$ is known, while $\mathbf{J}$ and $\mathbf{M}$ represent unknown surface currents, to be solved for.

Substituting (7.4)–(7.7) into (7.2) and (7.3), and the resulting expressions into (7.9), we arrive at the coupled set of integral equations

$$\begin{aligned} & j\omega\mu_n \int_S \mathbf{J}(\mathbf{r}\,')G_n(\mathbf{r}, \mathbf{r}\,')\,\mathrm{d}S' - \\ & -\frac{j}{\omega\varepsilon_n}\nabla \int_S \nabla'_S \cdot \mathbf{J}(\mathbf{r}\,')G_n(\mathbf{r}, \mathbf{r}\,')\,\mathrm{d}S' + \\ & +\nabla \times \int_S \mathbf{M}(\mathbf{r}\,')G_n(\mathbf{r}, \mathbf{r}\,')\,\mathrm{d}S' \end{aligned} = \begin{cases} \left[\mathbf{E}^{inc}\right]_{tan} & , \mathrm{n} = 1, \\ 0 & , \mathrm{n} = 2. \end{cases} \tag{7.10}$$

Following some mathematical manipulations on the second and third integral of (7.10), the nabla operator can be transferred to the Green's function leading to

$$\begin{aligned} & j\omega\mu_n \int_S \mathbf{J}(\mathbf{r}')G_n(\mathbf{r},\mathbf{r}')\,\mathrm{d}S' - \\ -\frac{j}{\omega\varepsilon_n} & \int_S \nabla'_S \cdot \mathbf{J}(\mathbf{r}')\nabla G_n(\mathbf{r},\mathbf{r}')\,\mathrm{d}S' + \\ & + \int_S \mathbf{M}(\mathbf{r}') \times \nabla' G_n(\mathbf{r},\mathbf{r}')\,\mathrm{d}S' \end{aligned} = \begin{cases} \left[\mathbf{E}^{inc}\right]_{tan} & , \mathrm{n} = 1, \\ 0 & , \mathrm{n} = 2, \end{cases} \tag{7.11}$$

where the property for the Green's function gradient, $\nabla G_n(\mathbf{r},\mathbf{r}') = -\nabla' G_n(\mathbf{r},\mathbf{r}')$, is used in (7.11).

7.2.1 Numerical Solution

For complex geometry of surface S, such as the human brain, the coupled integral equations set (7.11) cannot be solved analytically, hence the numerical approach is necessary. The corresponding numerical solution is carried out via the method of moments (MoM). It is a technique for finding an approximate solution to the system of a linear operator equations. Inserting the approximated function back into the operator equation, while multiplying it by a set of a known test functions, leads to a system of a linear equations. Solving the matrix system, one obtain the unknown coefficients from which equivalent surface currents are determined.

This work features an efficient MoM scheme in which the equivalent electric and magnetic currents $\mathbf{J}$ and $\mathbf{M}$ in (7.11), are first expanded by a linear combination of basis functions $\mathbf{f}_n$ and $\mathbf{g}_n$, respectively [5]

$$\mathbf{J}(\mathbf{r}) = \sum_{n=1}^{N} J_n \mathbf{f}_n(\mathbf{r}), \tag{7.12}$$

$$\mathbf{M}(\mathbf{r}) = \sum_{n=1}^{N} M_n \mathbf{g}_n(\mathbf{r}), \tag{7.13}$$

where J_n and M_n are unknown coefficients, and N is the number of elements used to discretize the surface S.

The brain surface S is discretized using the triangular elements or patches enabling one to use the Rao-Wilton-Glisson (RWG) basis functions [18] specially developed for triangular patches.

RWG function $\mathbf{f}_n$ is defined on T_n^+ and T_n^- pair of triangles that share a common edge (hence, sometimes the name edge-element is used), while on the rest of the surface S function vanishes.

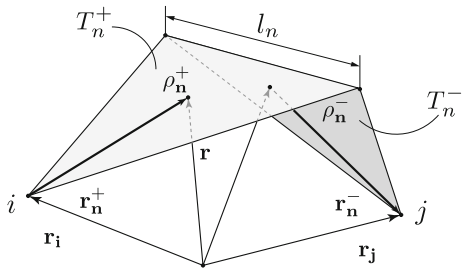

Fig. 7.2 RWG basis function $\mathbf{f}_n(\mathbf{r})$ defined on a pair of triangles in $\mathbf{R}^3$ [18]

Namely, the function is given by

$$\mathbf{f}_n^{\pm}(\mathbf{r}) = \begin{cases} \dfrac{l_n}{2A_n^{\pm}}\boldsymbol{\rho}_n^{\pm} & , \mathbf{r} \in T_n^{\pm}, \\ 0 & , \mathbf{r} \notin T_n^{\pm}, \end{cases} \tag{7.14}$$

where l_n is the edge length at the interface of triangles T_n^+ and T_n^-, while A_n^+ and A_n^- are the surface areas of those triangles. The vector $\boldsymbol{\rho}_n^+ = \mathbf{r} - \mathbf{r}_n^+$ is directed from the free vertex of T_n^+ and $\boldsymbol{\rho}_n^- = \mathbf{r}_n^- - \mathbf{r}$ is directed to the free vertex of T_n^-, as shown on Fig. 7.2.

While the surface electric current $\mathbf{J}$ is approximated by the RWG function $\mathbf{f}_n$, the surface magnetic current $\mathbf{M}$ is approximated by $\mathbf{g}_n = \hat{n} \times \mathbf{f}_n$, i.e. the function point wise orthogonal to the RWG function. The unknown equivalent currents $\mathbf{J}(\mathbf{r}')$ and $\mathbf{M}(\mathbf{r}')$ from (7.11) are substituted by (7.12) and (7.13). Equation (7.11) is next multiplied by the set of a test functions $\mathbf{f}_m$, where $\mathbf{f}_m = \mathbf{f}_n$, and integrated over the surface S. After some mathematical manipulations, it follows

$$\begin{aligned} & j\omega\mu_i \sum_{n=1}^{N} J_n \int_S \mathbf{f}_m(\mathbf{r}) \cdot \int_{S'} \mathbf{f}_n(\mathbf{r}')G_i \, dS' \, dS + \\ & + \frac{j}{\omega\varepsilon_i} \sum_{n=1}^{N} J_n \int_S \nabla_S \cdot \mathbf{f}_m(\mathbf{r}) \int_{S'} \nabla'_S \cdot \mathbf{f}_n(\mathbf{r}')G_i \, dS' \, dS \pm \\ & \pm \sum_{n=1}^{N} M_n \int_S \mathbf{f}_m(\mathbf{r}) \cdot [\hat{n} \times \mathbf{g}_n(\mathbf{r}')] \, dS + \\ & + \sum_{n=1}^{N} M_n \int_S \mathbf{f}_m(\mathbf{r}) \cdot \int_{S'} \mathbf{g}_n(\mathbf{r}') \times \nabla' G_i \, dS' \, dS \end{aligned} = \begin{cases} \displaystyle\int_S \mathbf{f}_m(\mathbf{r}) \cdot \mathbf{E}^{inc} \, dS & , i = 1, \\ 0 & , i = 2, \end{cases} \tag{7.15}$$

where subscript i is now the index of the medium. The third and the fourth integrals on the left hand side of (7.15) represent the residual term and the Cauchy principal value, respectively, of the last integral from (7.11). The residual term is calculated in the limiting case when $\mathbf{r} \to \mathbf{r}'$.

After extracting the two sums, (7.15) can be written in the form of the following linear equations system

$$\sum_{n=1}^{N}\left(j\omega\mu_i A_{mn,i}+\frac{j}{\omega\varepsilon_i}B_{mn,i}\right)J_n+\sum_{n=1}^{N}\left(C_{mn,i}+D_{mn,i}\right)M_n=\begin{cases}V_m & ,i=1,\\ 0 & ,i=2,\end{cases} \tag{7.16}$$

or in the matrix form as

$$[\mathbf{Z}]\cdot\{\mathbf{I}\}=\{\mathbf{V}\}, \tag{7.17}$$

where $\mathbf{Z}$ and $\mathbf{V}$ represents the system matrix, and the source vector, respectively, while $A_{mn,i}$, $B_{mn,i}$, $C_{mn,i}$ and $D_{mn,i}$ represent the surface integrals calculated for each $m-n$ combination of basis and testing functions, respectively.

Solution to the (7.17) is a vector $\mathbf{I}$ containing the unknown coefficients J_n and M_n. From these coefficients, the equivalent surface electric and magnetic currents $\mathbf{J}$ and $\mathbf{M}$, respectively, placed on the surface S of the dielectric object, i.e. the human brain, can be determined from (7.12) and (7.13), respectively. Knowing these currents, the electric field can be determined at an arbitrary point in space, i.e. the electric field inside the human brain represented by parameters (ε_2, μ_2), can be calculated from the following integral expression:

$$\begin{aligned}\mathbf{E}_2(\mathbf{r})=&-j\omega\mu_2\int_S\mathbf{J}(\mathbf{r}')G_2(\mathbf{r},\mathbf{r}')\,dS'-\\&-\frac{j}{\omega\varepsilon_2}\int_S\nabla'_S\cdot\mathbf{J}(\mathbf{r}')G_2(\mathbf{r},\mathbf{r}')\,dS'-\\&-\int_S\mathbf{M}(\mathbf{r}')\times\nabla G_2(\mathbf{r},\mathbf{r}')\,dS'.\end{aligned} \tag{7.18}$$

Once obtained the electric field distribution inside the brain, the distribution of the SAR can be readily found using the following relation

$$SAR=\frac{\sigma}{2\rho}|\mathbf{E}|^2, \tag{7.19}$$

where σ and ρ are the electric conductivity and the brain tissue density, respectively. The SAR distribution can be latter used as the input information to the thermal part of the brain model.

7.3 Thermal Dosimetry Model

It is well known that two most important factors for sustaining biological system are the metabolism and the blood flow [14]. The complex network of blood vessels significantly complicates mathematical modeling of heat transfer in biological tissues, unless a distributed heat source or sink is assumed.

The most commonly used model taking the flow of blood in this manner is the Pennes bioheat transfer equation [15]

$$\nabla \cdot (\lambda \nabla T) + w\rho_b c_b (T_a - T) + Q_m + Q_{ext} = \rho C \frac{\partial T}{\partial t}. \tag{7.20}$$

According to (7.20) the temperature rise in the given volume of tissue is based on the energy balance between the conductive heat transfer, the heat generated due to metabolic processes Q_m, the heat loss (generation) due to blood perfusion, and the influence of external heat sources Q_{ext}. The volumetric perfusion rate is given by ω, ρ_b and c_b are the density and the specific heat capacity of blood, respectively, λ is the thermal conductivity of the tissue, while T_a is the temperature of the arterial blood.

The analytical solutions of the bioheat transfer equation (7.20) are limited to cases of relatively high degree of symmetry [21], thus making numerical approach necessary for problems with complex geometry of the domain arising for realistic exposure scenarios. In this work the problem of determining the temperature distribution in the human brain is addressed using the finite element method (FEM) [7].

The steady-state temperature distribution in the brain, exposed to an incident time harmonic EM field, is governed by the stationary form of the bioheat equation (7.20)

$$\nabla \cdot (\lambda \nabla T) + W_b c_b (T_a - T) + Q_m + Q_{ext} = 0 \tag{7.21}$$

extended with Q_{ext}. This term represents the amount of heat generated per unit time per unit volume due to absorption of EM energy in the biological tissue [4, 6, 7]:

$$Q_{ext} = \rho \cdot SAR, \tag{7.22}$$

where SAR is defined by (7.19).

The bioheat equation (7.21) is supplemented by the corresponding boundary conditions, as shown in Fig. 7.3.

This work features the use of Neumann or the natural boundary conditions given by

$$-\lambda \frac{\partial T}{\partial \hat{n}} = h_s (T - T_{amb}), \tag{7.23}$$

where, λ is the thermal conductivity of the brain, and h_s is the convection coefficient between the surface and the surroundings, T and T_{amb} are the surface and the ambient

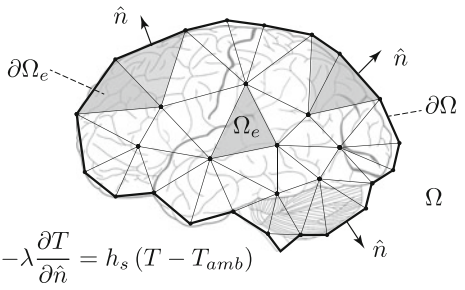

Fig. 7.3 Illustration of the finite element mesh with boundary conditions on the brain surface

temperature, respectively. Unit normal $\hat{n}$ is directed from the surface S, as shown on Fig. 7.3.

Note that the heat loss due to radiation, and the forced convection are neglected. Neverthless, (7.23) satisfactorily describes the heat exchange between the surface of the brain and the environment.

Since the human brain is separated from the scalp by various other tissues, when using the homogeneous brain model, it is necessary to account for the heat exchange through all of them. This is ensured by using the effective thermal convection coefficient h_{eff} [23] between the brain and the surroundings.

The widely adopted value for the effective thermal convection coefficient, typical for the human brain, is $h_{eff} = 1.2 \times 10^{-3}$ W/cm^2°C [20]. This value is used in our homogeneous thermal model of the brain, as well.

7.3.1 Finite Element Solution

The finite element formulation of (7.21) is based on the weighted residual approach. The approximate solution of (7.21) is expanded in terms of the known basis functions N_i and the unknown coefficients α_i

$$T(x, y, z) = \sum_{i=1}^{m} N_i(x, y, z)\alpha_i, \tag{7.24}$$

where i is the node index, m is the number of nodes per finite element, and N_i is the basis function given by

$$N_i(x, y, z) = \frac{1}{D}(V_i + a_i x + b_i y + c_i z), \quad i = 1, 2, 3, 4, \tag{7.25}$$

where expressions for the coefficients a_i, b_i, c_i, V_i and D can be found in [19].

Multiplying (7.21) by a set of weighting functions W_j and integrating over the domain $\Omega = V$, yields

$$\int_{\Omega} [\nabla \cdot (\lambda \nabla T) + W_b c_b (T_a - T) + Q_m + Q_{ext}] W_j \, \mathrm{d}\Omega = 0. \tag{7.26}$$

Applying the same procedure on (7.23), it follows

$$-\lambda \int_{\partial\Omega} \frac{\partial T}{\partial \hat{n}} W_j \, \mathrm{d}S = \int_{\partial\Omega} h_s T W_j \, \mathrm{d}S - \int_{\partial\Omega} h_s T_{amb} W_j \, \mathrm{d}S. \tag{7.27}$$

Taking the integration by parts in the first term of (7.26), the Gauss' divergence theorem is applied, resulting in

$$\int_{\Omega} \nabla \cdot \left[(\lambda \nabla T)\, W_j \right] \mathrm{d}\Omega = \lambda \int_{\partial\Omega} \frac{\partial T}{\partial \hat{n}} W_j \,\mathrm{d}S. \tag{7.28}$$

Inserting (7.28) into (7.26), and after some rearranging, a suitable expression for the FEM implementation is obtained [7]

$$\int_{\Omega} \lambda \nabla T \cdot \nabla W_j \,\mathrm{d}\Omega + \int_{\Omega} W_b c_b T W_j \,\mathrm{d}\Omega = \\ = \int_{\partial\Omega} \lambda \frac{\partial T}{\partial \hat{n}} W_j \,\mathrm{d}S + \int_{\Omega} (W_b c_b T_a + Q_m + Q_{ext}) W_j \,\mathrm{d}\Omega. \tag{7.29}$$

Having discretized the brain surface by triangular elements, performed in the electromagnetic part of the model [5], the interior of the brain depicted as Ω in Fig. 7.3 was discretized by the tetrahedral elements.

Implementing the Galerkin-Bubnov procedure, followed by the standard finite element discretization of (7.29), the weak formulation for the finite element domain Ω_e can be written in the matrix form

$$[K]^e \{T\}^e = \{M\}^e + \{P\}^e, \tag{7.30}$$

where $[K]^e$, $\{M\}^e$ and $\{P\}^e$ are the finite element matrix

$$[K]^e_{ji} = \int_{\Omega_e} \lambda^e \nabla W_i \cdot \nabla W_j \,\mathrm{d}\Omega_e + \int_{\Omega_e} W_b^e c_b^e W_i W_j \,\mathrm{d}\Omega_e, \tag{7.31}$$

the flux vector on the boundary $\partial\Omega_e$ of the finite element

$$\{M\}^e_j = \int_{\partial\Omega_e} \lambda^e \frac{\partial T}{\partial \hat{n}} W_j \,\mathrm{d}S_e, \tag{7.32}$$

and the finite element source vector

$$\{P\}^e_j = \int_{\Omega_e} (W_b^e c_b^e T_a + Q_m^e + Q_{ext}^e) W_j \,\mathrm{d}\Omega_e, \tag{7.33}$$

respectively.

Solving (7.31)–(7.33) for each N elements, the global matrix is assembled from the contribution of the local finite element matrices, while the global flux and the source vectors are assembled from the local flux and the local source vectors, respectively:

$$[K]\{T\} = \{M\} + \{P\}. \tag{7.34}$$

The solution of the matrix system (7.34) is the vector $\{T\}$ whose elements represent the values of temperature in the tetrahedra nodes.

7.4 Computational Example

The numerical results for our homogeneous three-dimensional brain model are presented in this section. The dimensions of the average adult human brain are used (length 167 mm, width 140 mm, height 93 mm, volume of 1400 cm^3) [2]. The surface of the brain is disretized using the $T = 696$ triangular elements and $N = 1044$ edge-elements, while the interior of the brain is discretized using 1871 tetrahedral elements. The frequency dependent parameters of the human brain are taken from [8]. The value for the relative permittivity and the electrical conductivity of the brain are $\varepsilon_r = 45.805$ and $\sigma = 0.766$ S/m, respectively, taken as the average values between white and gray matter at 900 MHz. Value for the density of the brain tissue is $\rho = 1046$ kg/m^3.

The incident plane wave of power density of $P = 5$ mW/cm^2 is directed perpendicular to the right side of the brain (positive x coordinate), the polarization of the wave is in the horizontal (y coordinate) direction, while the operating frequency is 900 MHz.

Using our EM model based on the SIE formulation [5], the distribution of the electric and magnetic fields on the brain surface, shown on Fig. 7.4, are determined first.

From the electric field values in the brain interior, SAR can be calculated using (7.19). The obtained peak and average SAR values are 0.856 W/kg and 0.174 W/kg, respectively. The calculated results show that the peak SAR value in the human brain does not exceed the limit set by ICNIRP [11] as a basic restriction for localized SAR (in the head and the trunk), for the occupational exposure (10 W/kg). Figure 7.5 shows the distribution of the SAR obtained for the brain model.

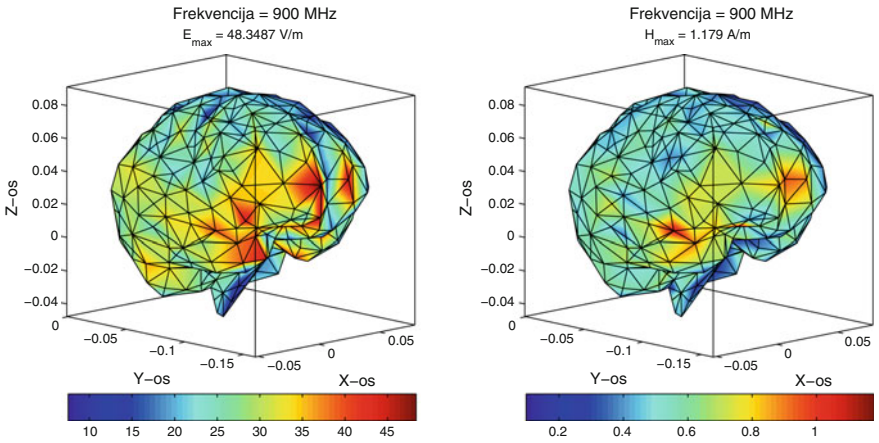

Fig. 7.4 Distribution of electric and magnetic fields on the brain surface. Horizontally polarized plane wave of frequency 900 MHz

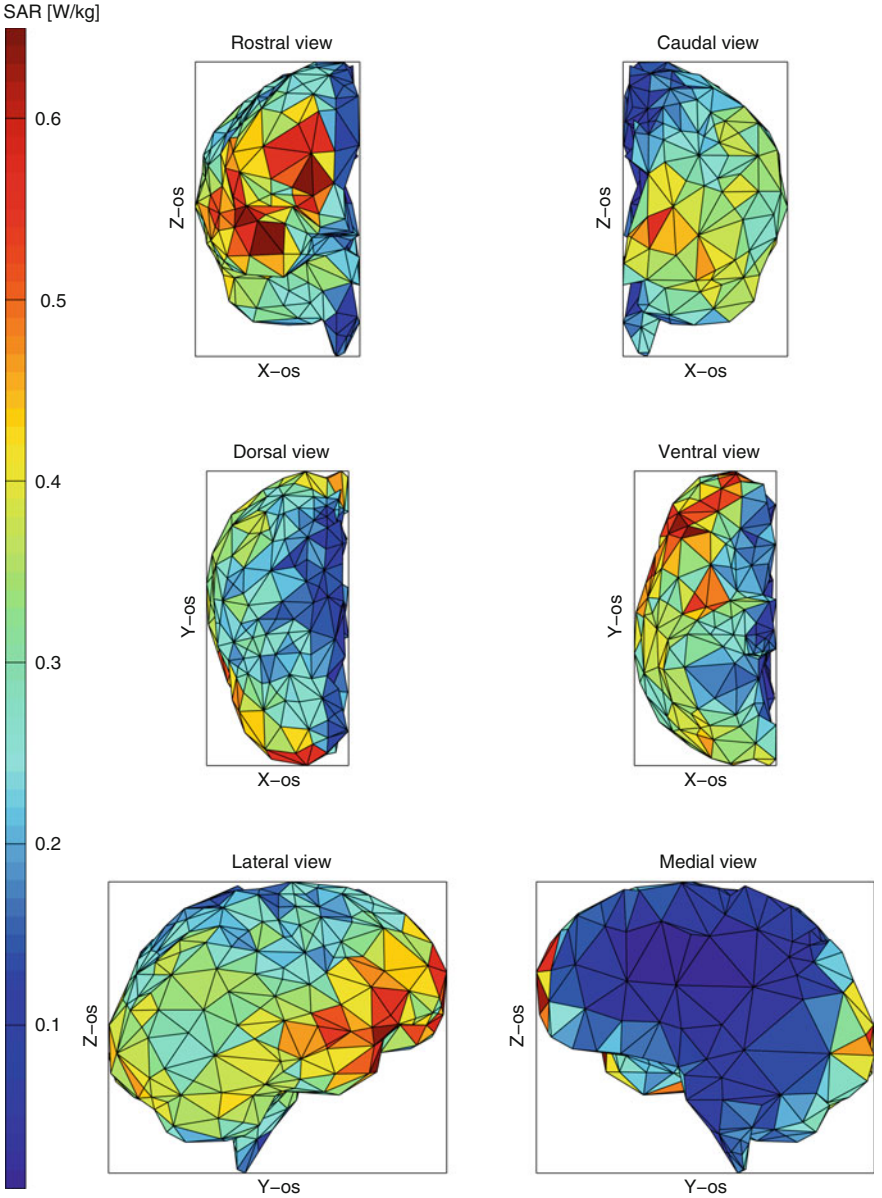

Fig. 7.5 Distribution of SAR for the case of horizontally polarized plane wave of frequency 900 MHz, power density $P = 5$ mW/cm^2

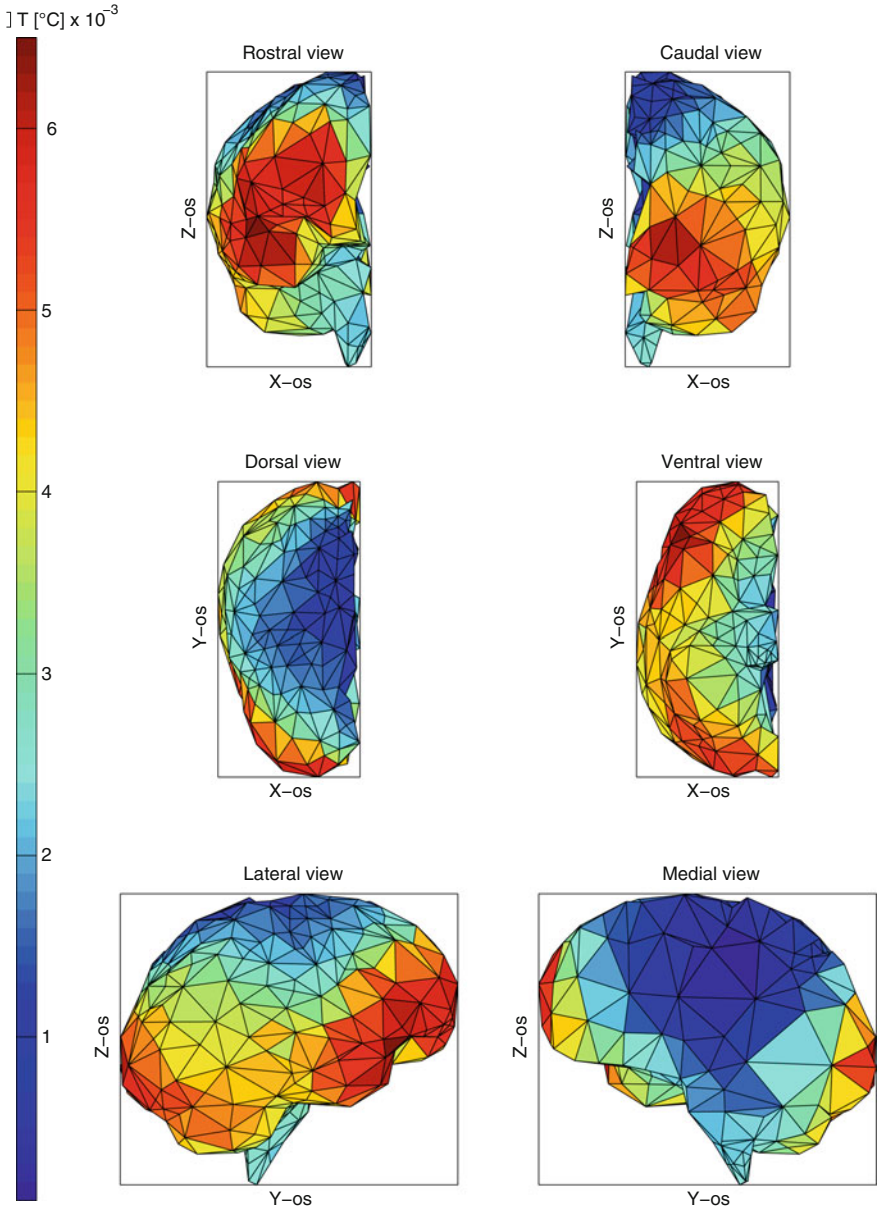

Fig. 7.6 Temperature rise in the human brain model due to incident 900 MHz horizontally poralized plane wave, power density $P = 5\,\mathrm{mW/cm^2}$

The human brain parameters used in the thermal dosimetry model are taken from [13]: the heat conductivity $\lambda = 0.513$ W/m °C, the volumetric perfusion rate of blood $W_b = 33297$ kg/m^3, the specific heat capacity of blood $c_b = 1$ J/kg °C, the heat generated due to metabolism $Q_m = 6385$ W/m^3, and the arterial blood temperature $T_{art} = 37$ °C.

Figure 7.6 shows the results for the temperature rise in the human brain. The maximum temperature rise is $\Delta T = 7.11 \times 10^{-3}$ °C, which is rather negligible compared to the values proven to cause adverse health effects.

7.5 Conclusion

This work deals with the electromagnetic–thermal dosimetry model for the human brain exposed to EM radiation. The electromagnetic model based on the surface integral equation formulation is first derived from the equivalence theorem and using the boundary conditions for the electric field. The human brain is represented by an arbitrarily shaped lossy homogeneous dielectric. The thermal model of the brain is based on the extended form of the Pennes' bioheat equation supplemented by the natural boundary condition on the brain surface. The numerical results for the electric and magnetic fields are presented for the brain exposed to a radiation of 900 MHz horizontally polarized plane wave. The calculated peak SAR value in the human brain does not exceed the basic restriction for the occupational exposure set by the ICNIRP. Also, the resulted temperature rise in the human brain is rather negligible compared to established health based threshold.

References

1. Adair, E.R., Petersen, R.: Biological effects of radiofrequency/microwave radiation. IEEE Trans. Microw. Theory Tech. **50**(3), 953–962 (2002). doi:10.1109/22.989978
2. Blinkov, S.M., Glezer, I.I.: The Human Brain in Figures and Tables: A Quantitative Handbook. Plenum Press, New York (1968)
3. Chew, W.C., Tong, M.S., Hu, B.: Integral Equation Methods for Electromagnetic and Elastic Waves. Morgan & Claypol Publishers, California (2009)
4. Cvetković, M., Čavka, D., Poljak, D., Peratta, A.: 3D FEM temperature distribution analysis of the human eye exposed to laser radiation. Adv. Comput. Methods Exp. Heat Transf. XI. WIT Trans. Eng. Sci. **68**, 303–312 (2009)
5. Cvetković, M., Poljak, D.: An efficient integral equation based dosimetry model of the human brain. In: Proceedings of the International Symposium on Electromagnetic Compatibility (EMC EUROPE) 2014, Gothenburg, Sweden, 1–4 September, pp. 375–380 (2014)
6. Cvetković, M., Poljak, D., Peratta, A.: Thermal modelling of the human eye exposed to laser radiation. In: Proceedings of 2008 International Conference on Software, Telecommunications and Computer Networks, Split, Croatia, 25–26 September, pp. 16–20 (2008)
7. Cvetković, M., Poljak, D., Peratta, A.: FETD computation of the temperature distribution induced into a human eye by a pulsed laser. Prog. Electromagn. Res. PIER **120**, 403–421 (2011)

8. Gabriel, C.: Compilation of the dielectric properties of body tissues at RF and microwave frequencies. Technical report, Brooks Air Force Base, TX. Report: AL/OE-TR-1996-0037 (1996)
9. Harrington, R.: Boundary integral formulations for homogeneous material bodies. J. Electromagn. Waves Appl. **3**(1), 1–15 (1989)
10. Hirata, A., Shiozawa, T.: Correlation of maximum temperature increase and peak SAR in the human head due to handset antennas. IEEE Trans. Microw. Theory Tech. **51**(7), 1834–1841 (2003). doi:10.1109/TMTT.2003.814314
11. International Commission on Non-Ionizing Radiation Protection: ICNIRP): Guidelines forlimiting exposure to time-varying electric, magnetic and electromagnetic fields (up to 300GHz). Health Physics **74**(4), 494–522 (1998)
12. International Commission on Non-Ionizing Radiation Protection: ICNIRP): Guidelines forlimiting exposure to time-varying electric and magnetic fields (1 Hz to 100 kHz). Health Physics **99**(6), 818–836 (2010). doi:10.1097/HP.0b013e3181f06c86
13. McIntosh, R.L., Anderson, V.: A comprehensive tissue properties database provided for the thermal assessment of a human at rest. Biophys. Rev. Lett. **5**(3), 129–151 (2010)
14. Minkowycz, W.J., Sparrow, E.M., Murthy, J.Y.: Handbook of Numerical Heat Transfer, 2nd edn. Wiley, New York (2006)
15. Pennes, H.H.: Analysis of tissue and arterial blood temperatures in the resting human forearm. 1948. J. Appl. Physiol. **85**(1), 5–34 (1998)
16. Poggio, A.J., Miller, E.K.: Integral equation solutions of three–dimensional scattering problems. In: Mittra, R. (ed.) Computer Techniques for Electromagnetics, Second Edition, Chap. 4, pp. 159–264. Hemisphere Publishing Corporation, Washington (1987)
17. Poljak, D., Peratta, A., Brebbia, C.A.: The boundary element electromagnetic-thermal analysis of human exposure to base station antennas radiation. Eng. Anal. Bound. Elem. **28**(7), 763–770 (2004). doi:10.1016/j.enganabound.2004.02.004
18. Rao, S., Wilton, D.R., Glisson, A.: Electromagnetic scattering by surfaces of arbitrary shape. IEEE Trans. Antennas Propag. **30**(3), 409–418 (1982)
19. Silvester, P.P., Ferrari, R.L.: Finite Elements for Electrical Engineers, 3rd edn. Cambridge University Press, Cambridge (1996)
20. Sukstanskii, A., Yablonskiy, D.: Theoretical model of temperature regulation in the brain during changes in functional activity. Proc. Natl. Acad. Sci. **103**(32), 12144–12149 (2006). doi:10.1073/pnas.0604376103
21. Sukstanskii, A.L., Yablonskiy, D.A.: An analytical model of temperature regulation in human head. J. Therm. Biol. **29**(7), 583–587 (2004). doi:10.1016/j.jtherbio.2004.08.028
22. Umashankar, K., Taflove, A., Rao, S.: Electromagnetic scattering by arbitrary shaped three-dimensional homogeneous lossy dielectric objects. IEEE Trans. Antennas Propag. **34**(6), 758–766 (1986)
23. Zhu, M., Ackerman, J.J.H., Sukstanskii, A.L., Yablonskiy, D.A.: How the body controls brain temperature: the temperature shielding effect of cerebral blood flow. J. Appl. Physiol. **101**(5), 1481–1488 (2006). doi:10.1152/japplphysiol.00319.2006